

Retroreflective shadowgraph technique for large-scale flow visualization

Michael J. Hargather* and Gary S. Settles

Gas Dynamics Laboratory, Pennsylvania State University, 301D Reber Building, University Park, Pennsylvania 16802, USA

*Corresponding author: mjh340@psu.edu

Received 28 May 2009; accepted 30 June 2009;
posted 15 July 2009 (Doc. ID 112071); published 27 July 2009

A simple and robust retroreflective shadowgraph technique is presented for the visualization of refractive phenomena across a broad range of scales in space and time. Originally developed by Edgerton, it is improved here with techniques for producing coincident shadowgram illumination. The optical components required to construct a simple system are discussed, including the retroreflective screen material. The optical sensitivity of the system is explored for visualization of shock waves and turbulent eddies. The shadowgraph system is used here to visualize experiments performed in the laboratory, on a military test range, and in an open field. © 2009 Optical Society of America

OCIS codes: 000.2170, 120.5710.

1. Introduction

Traditional schlieren techniques [1] are almost never applied to large-scale experiments. Achieving a large field of view requires a different approach, such as lens-and-grid schlieren [1,2] or background-oriented schlieren [3]. Although these methods are useful for large-scale flow visualization, the simple shadowgraph can often provide the most robust solution for large fields of view.

Shadowgraphy as a flow visualization method was invented around 1672 by Robert Hooke, using only the Sun and a white surface upon which to cast the shadow [1]. The modern “direct” shadowgraph technique differs from this mainly in the use of improved light sources, cameras, and screens upon which to cast the shadow. Harold E. “Doc” Edgerton (1903–1990), the pioneer of the electronic strobe, advanced the technique significantly in 1958 with his flashlamp [4] and an elegant approach to direct-shadowgraph imaging of explosions and gunshots [5]. His approach required only a retroreflective screen, strobe illumination, and an old-fashioned

view camera. To demonstrate robustness, Edgerton photographed the shadowgram of a blasting-cap explosion outdoors in daylight (see Fig. 6.14a of [1]). One limitation in Edgerton’s approach, however, was the noncoaxial light source and camera, which resulted in double-imaging of solid objects in the field of view. This problem was solved by the use of a beam splitter during ballistic research at the German–French Institut Sant-Louis (ISL) and the Krupp Firing Range in Germany [6].

The retroreflective shadowgraph technique was reinvented by Parthasarathy *et al.* [7] as a method of visualizing helicopter rotor tip vortices. Although they did not cite Edgerton’s precedent, their “wide-field shadowgraphy” was nonetheless a proper use of Edgerton shadowgraphy, utilizing its simplicity, high gain, high speed, and robustness in the field. A number of subsequent rotor tip vortex investigations by various investigators followed suit [8,9].

More recent approaches have favored background-oriented schlieren (BOS) [3] rather than shadowgraphy for large-scale flow visualizations. Using image processing routines, two images of a background pattern, one with a schlieren object and one without, can be compared to determine density gradients within the schlieren object from the

apparent shift in the background pattern [10,11]. Meier first proposed using this technique for large-scale flow visualization when he suggested using natural backgrounds, such as distant trees or mountains, in his original patent [3]. Richard and Raffel, however, were the first to use “natural” backgrounds such as white paint splatter on concrete and a grassy field to visualize compressible vortices from helicopter rotors [12]. Hargather and Settles recently used the BOS technique for large-scale outdoor flow visualization of thermal plumes, explosions, and gunshots [13]. Their results include a comparison of lens-and-grid schlieren imaging and the BOS technique, which concludes that BOS is not as sensitive nor as visually appealing as a high-quality schlieren or shadowgraphy image.

The present research reconsiders the classical “Edgerton” retroreflective shadowgraphy with the addition of modern scientific equipment to develop a robust portable technique for large-scale indoor and outdoor flow visualization. A range of optical configurations is presented. The shadowgraph sensitivity and recommended geometric configurations are also discussed while illustrating several high- and low-speed applications.

2. Experimental Methods

A. Principles of Direct Shadowgraphy

Direct shadowgraphy with diverging illumination is elegantly simple in its governing principles and optical sensitivity. As sketched in Fig. 1, the basic setup requires only a light source, a camera, and a screen on which to cast a shadow. A “point” source of light L , at a distance h from the screen, projects a spot of height d' . Refractive disturbances in the schlieren object, S , bend light rays from their original paths, casting a shadow pattern on the screen. The optical sensitivity of this shadowgraph system is near its maximum when S is located within the range $0.3 < g/h < 0.7$ [1]. Since S is thus roughly halfway between the light source and screen, the diameter d of the field of view can be roughly half that of the screen, d' .

The purpose of the camera in Fig. 1 is to photograph the shadowgram that forms on the screen. If

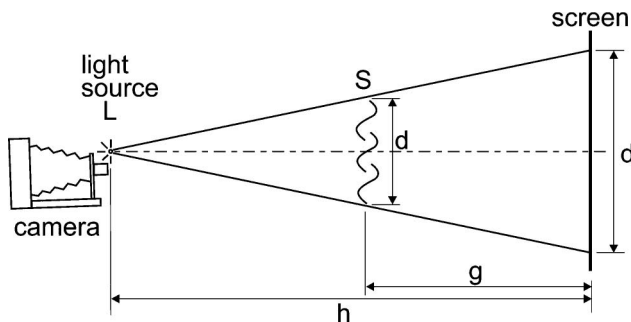


Fig. 1. Diagram of Edgerton’s direct shadowgraph technique. Note that the camera is off-axis with respect to the light source, resulting in a double shadow in the image.

the camera is slightly offset laterally from the light source, as described by Edgerton [4,5] and shown here, then solid objects within S will be slightly double imaged in the resulting shadowgram, as shown in Fig. 2. This problem is solved here with the newly proposed optical alignments described below. Note that the screen, whether retroreflective or not, does not act as a mirror that reflects light back to the source, but rather acts as a surface upon which the shadow is cast. As a result of this, the camera placement is relatively arbitrary so long as the desired shadowgram is captured, with best results generally obtained when the camera is coincident with the light source. Also note that there are some scenarios wherein the noncoincident alignment may be desired to separate the shadowgram from the direct image of an object [Fig. 2(a)], but these are not considered here.

Direct shadowgraphy visualizes the Laplacian of the refractive field; thus thin, sharp refractive disturbances are best shown. The technique lends itself well to visualizing shock waves and turbulent eddies but fails to capture more-gradual disturbances such as Prandtl–Meyer fans, which are better revealed by the schlieren method.

In the direct shadowgraph technique, the shadow of the schlieren object is projected onto the screen where the camera images it. Direct shadowgraphy first requires point-source illumination to produce undistorted shadows on the screen. The camera must then be sharply focused on the screen. If the camera lens does not allow a sufficiently large depth of field, the schlieren object itself can be slightly defocused, while the shadow remains in focus. This results in

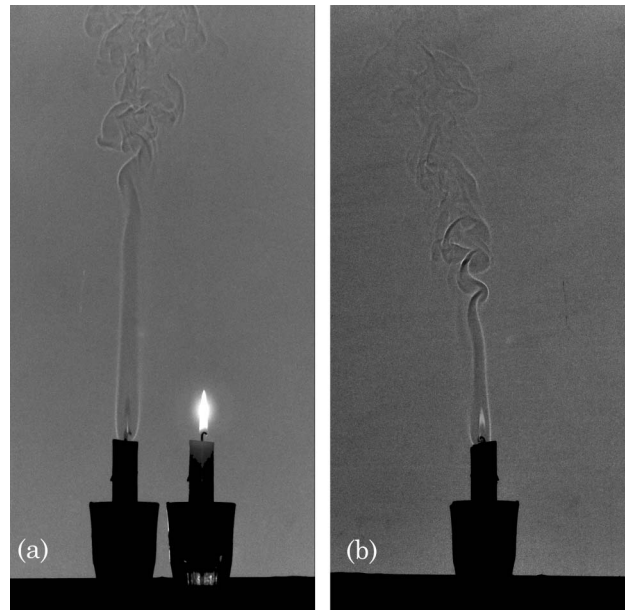


Fig. 2. Shadowgrams of a candle plume from (a) Edgerton’s non-coincident configuration and (b) from a coincident setup. The non-coincident configuration (a) results in both the actual object and its shadow being present in the image. The physical candle is on the right within frame (a), and the shadowgram is on the left.

poor photography if the subject is out of focus, and can lead to a distorted shadowgram if the subject is sufficiently defocused. For a more complete review of direct shadowgraphy the reader is directed to Chapter 6 of [1].

B. Coincident Optical Configurations for Direct Shadowgraphy

The first and simplest solution to producing coincident illumination is to use a beam splitter as shown in Fig. 3(a). This setup does not require precise alignment of components, with the exception of the camera. The camera must be positioned so that it can image the screen and so that it is in line with the physical object; otherwise, a double image can occur. The alignment procedure is simple for qualitative use and simply requires positioning the camera so that the shadowgram and schlieren object align appropriately. For quantitative purposes, however, this simple alignment could potentially produce errors. Although its alignment is not critical, the light source must still be focused to a point; the location of the focus relative to the beam splitter is immaterial.

One difficulty with this configuration [Fig. 3(a)] is that the beam splitter causes a loss of approximately 3/4 of the available light. This loss is most significant for high-speed applications where submicrosecond exposures are desired. The loss can be compensated by increasing the light source strength, although this can be problematic when considering a field-portable system. The semitransparent nature of the beam splitter can also result in the camera imaging both the screen and the field behind the beam splitter. A black backdrop is therefore recommended behind the beam splitter on the optical axis of the camera.

The second configuration shown in Fig. 3(b) uses a mirror with a small spot of the silvered back removed. This configuration requires that the light source is precisely and sharply focused upon this spot on the mirror surface in order to pass the maximum amount of light. The hole must be small: a 1–2 mm hole was used here, in order to not be observed in the final image, with the camera focused at or near infinity. The camera must also be properly aligned to prevent the double imaging as described above.

Figure 3(c) shows a third option for coincident illumination, using a small “rod mirror” mounted on a clear glass filter that fits over the camera lens. The rod mirror, as used here, is a cylindrical rod with

a mirrored surface cut at a 45° angle to the camera axis. The rod mirror is aligned with the center of the lens, and thus also with the camera axis. The light source is sharply focused on this rod mirror using a simple lens. The rod mirror then projects the illumination onto the retroreflective screen. Again, because the lens is focused at infinity, the region occluded by the rod mirror is insignificant and therefore does not materially interfere with the image. This method provides the least light losses and eliminates the possibility of a double image; it is therefore the approach used here for all high-speed and quantitative purposes.

C. Retroreflective Screen

In principle, a direct shadowgraph system requires only a simple diffuse white screen on which a shadow can be cast [1]; in practice, a retroreflective screen material is preferred because it is capable of returning orders of magnitude greater illumination to the camera than a diffuse screen. For high-speed shadowgraphy, this light intensity gain is essential. The retroreflective screen functions crudely like a spherical reflector, returning the majority of the incident light to the vicinity of its point of origin.

The retroreflective material used here is 3M Scotchlite 7610, a high-gain, industrial-grade, exposed-lens, diffuse gray retroreflective plastic-based sheet material [14]. Only 0.1 mm thick, its backside is precoated with a pressure-sensitive adhesive and covered with a removable protective liner. The manufacturer claims a 900× luminance factor compared with a plain white diffuse screen. This and other details of Scotchlite 7610 performance versus that of other retroreflective materials were examined by Winburn *et al.* [15]. The primary screen used here is approximately 2.4 m square and is mounted to a rigid aluminum frame for stability.

D. Cameras and Light Source

The purpose of the camera in the direct shadowgraphy technique is to record an image of the shadow that forms on the screen. For high-speed imaging, a Photron APX-RS digital camera is used here, although any similar modern digital video camera would serve as well. This camera is capable of recording at frame rates up to 250,000 frames per second (fps) with an independently controlled shutter, which is typically set at 1 μs exposure. The resolution of this camera decreases with increasing frame rate: the

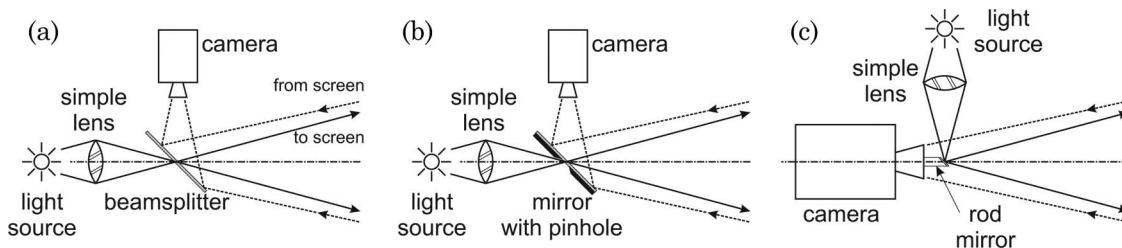


Fig. 3. Diagrams of the coincident illumination setups for retroreflective shadowgraphy, using (a) a beam splitter, (b) a mirror with a “pinhole,” and (c) a rod mirror.

maximum resolution of 1024×1024 pixels is only available up to 3000 fps, while at 250,000 fps the resolution is only 16×128 pixels.

For low-speed imaging, a Nikon D90 digital camera is used. This camera records 12.3 megapixel still images with the added capability of recording high-definition-quality (HD) video at 24 fps. The exposure and lens settings used for the Nikon camera are set as required for good photography and in general vary based on the schlieren disturbance being visualized.

The light source required for retroreflective shadowgraphy must be small and bright, but otherwise is dependent solely on the object being imaged and the desired exposure. For high-speed applications, a 1000 W xenon arc lamp from the Newport Corporation was used, which is focused to a point using a simple lens. This self-contained light source is found to be appropriate to produce sufficient light for $1 \mu\text{s}$ exposure, but is also found to be sensitive to high temperature and humidity conditions outside of the laboratory, requiring active external cooling to function properly. The continuous arc lamp offers the convenience of high-speed imaging without the need for flash synchronization. However, some applications may require greater illumination, for which a synchronized flash lamp will be required [4]. For low-speed applications the light source requirements are less stringent, typically the same light source used here, resulting in short exposure times on all images.

3. Experimental Results

A. Explosion Shadowgraphy: Laboratory Experiments

This shadowgraph technique can be used to study explosive charges and shock propagation. Recent work by Kleine *et al.* [16] and Hargather and Settles [17] has investigated the TNT equivalence of laboratory-scale explosive charges using focused shadowgraph techniques. Hargather and Settles [17] used a z-type focused shadowgraph system to measure shock radius as a function of time and a retroreflective shadowgraph technique to verify the sphericity of their explosions. The retroreflective shadowgraph technique can also be used to measure shock radius as a function of time.

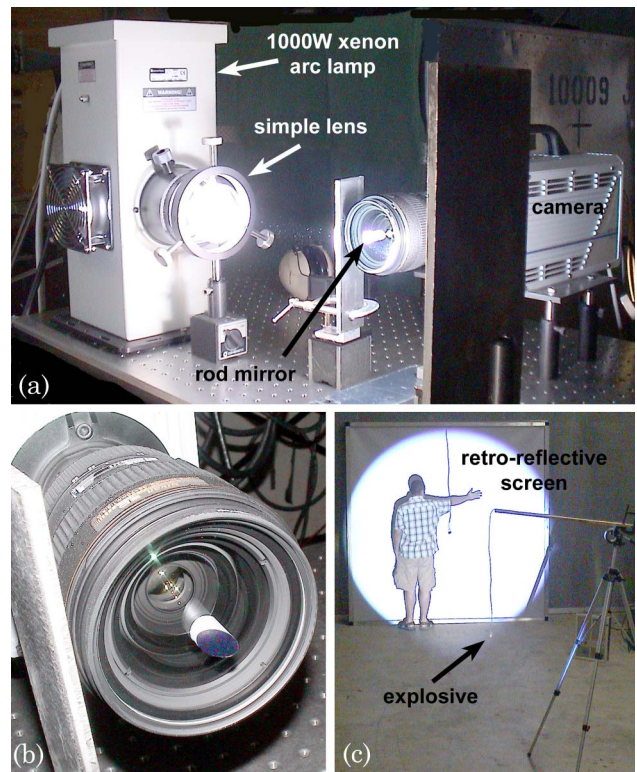


Fig. 4. (Color online) (a) Oblique side view of the camera/illuminator assembly, with vertical plates used as beam stops. (b) APX-RS digital camera with a 20–70 mm Nikon zoom lens and the rod mirror mounted on a clear lens filter. (c) An explosive charge is suspended by a wire in the foreground while the author (MJH) stands before the retroreflective screen in the background, on which the shadowgram of the suspended charge can be observed.

For these experiments the rod–mirror optical set-up was used, as shown in Fig. 4. The screen was approximately 10 m from the camera–illuminator assembly, and the explosive charge was suspended approximately halfway between the screen and camera.

A series of images showing the explosion of a 1 g triacetone triperoxide (TATP) charge is shown in Fig. 5. The images are $100 \mu\text{s}$ apart, each recorded with a $1 \mu\text{s}$ exposure. The rightmost two images show the full available resolution (512×512 pixels), while the others were cropped for display purposes. These

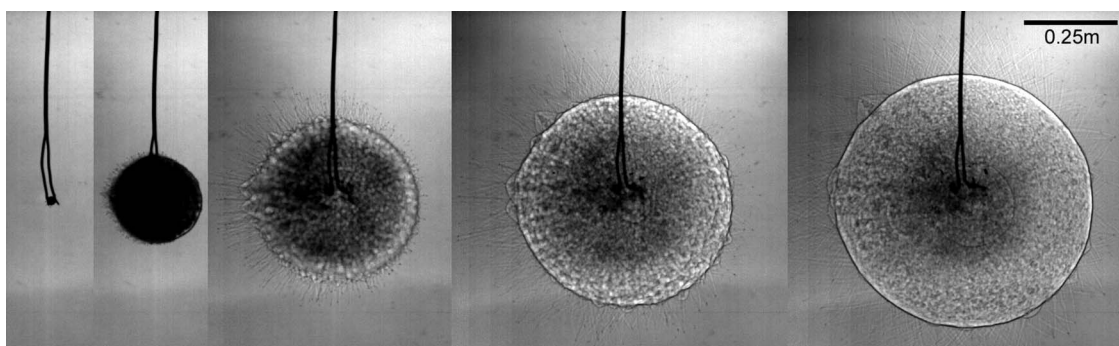


Fig. 5. Digital image series showing shadowgrams of a 1 g TATP explosion.

images show a highly spherical shock propagation with some fragments of binder material also being projected from the explosion. The turbulence caused by the shock propagation and the expansion of the explosive products is clearly visible in these images. The quantitative data of the shock radius versus time for this explosion are not presented here, but are elsewhere [17,18].

One complication with using a retroreflective shadowgraph technique for quantitative shock wave measurements is the need to perform a correction for the geometry associated with the divergent light. The geometry correction was described by Dewey [19] and is shown here in Fig. 6. This correction is required because the shock wave will only be visible where it is perpendicular to the illuminating light rays. The diverging light of the retroreflective technique results in a different plane of the explosion being visualized at each succeeding instant. The apparent path of the shock front will thus be an arc centered between the explosion center and the camera. This simple correction requires only basic geometric calculations for most laboratory-scale experiments, but is necessary for the accuracy of quantitative measurements.

B. Explosion Shadowgraphy: Large-Scale Outdoor Experiments

The divergent light source further complicates the data collection and analysis as the explosion source is displaced from the optical axis. This is possible in large-scale experiments, and is shown schematically in Fig. 7. Again the shock is visible only when its propagation, and thus its refractive index gradient, is perpendicular to the illuminating light rays. For a near-field, off-axis explosion, the visualized shock front will continue to follow the arc defined by its location relative to the camera, as stated above. In the limit of a far-field explosion that produces a planar shock wave at the measurement location, the shock only becomes sharply visible at a single specific location within the field of view where parallelism with the illuminating light rays exists, and is weakly visible near this point.

The visualization of a far-field explosion was performed outdoors using the present retroreflective shadowgraph system during a holiday fireworks display. The shadowgraph system was set up with the retroreflective screen approximately 15 m from the

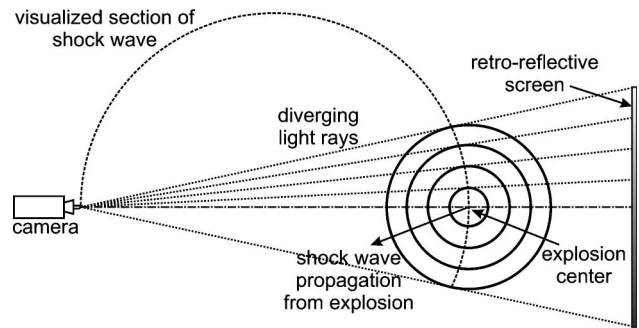


Fig. 6. Schematic highlighting the geometric correction required when analyzing retroreflective shadowgrams of a spherical shock wave. The shock wave will be visible only when it is perpendicular to the diverging light rays from the source.

light source. The optical axis of the system was approximately 150 m from the launch site of the fireworks, with the optical axis perpendicular to the expected propagation of the shock waves produced by the fireworks explosions. The 10 and 15 cm diameter fireworks shells exploded 130–200 m above the ground, resulting in expected shock wave angles of approximately 45° at the shadowgraph location.

Figure 8 shows a series of shadowgrams recorded for one fireworks explosion. The images are $100\ \mu\text{s}$ apart, each recorded with a $2\ \mu\text{s}$ exposure. The series clearly shows a segment of the spherical shock wave transitioning from being weakly focused to sharply focused, then back to weakly focused, as it transits the location where its propagation is perpendicular to the illuminating light rays. The location at which the shock appears sharp within the shadowgram is relatively random, based on the point in space where the fireworks exploded relative to the optical axis. Shock waves were visible in the digital images for all 14 observed fireworks explosions, but their locations within the shadowgrams varied. The shock impingement angle also does not correlate well with the fireworks explosion height due to the three-dimensional location variability relative to the optical axis.

Figure 8 highlights the robustness of this optical system as well as some potential problems that can be encountered in the field. This retroreflective shadowgraph system is robust enough to be transported to a remote location, where it can be set up and powered by a commercial gasoline-powered electrical generator. The optical performance of the

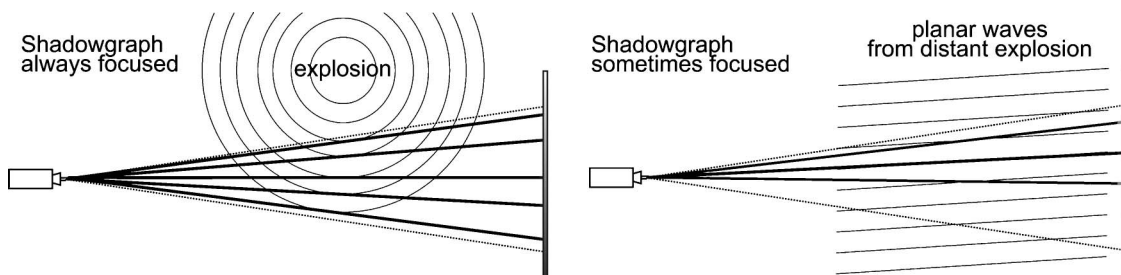


Fig. 7. Schematic of the visibility of the shock waves produced by explosions located off the optical axis.

system is not hindered, in general, by the outdoor conditions. The APX-RS camera used is well suited to the outdoor environment and is unaffected by typical adverse conditions. The screen material is robust and unaffected by direct sunlight; however, it is susceptible to degraded performance if it becomes wet. In the present experiments, conducted on a typical summer night in central Pennsylvania, a portion of the screen became fogged with condensation from the cool night air. The regions on the screen where condensation occurred appear as dark spots in Fig. 8 because the retroreflective gain of the screen is degraded by the water droplets. The condensation zone, which occurred at the boundary of the supporting structure behind the screen, is identified in the leftmost image of Fig. 8.

Outdoor experiments can also be affected by local flora and fauna. The present experiments proved especially attractive to insects, which were frequently captured in shadowgrams, as also indicated in Fig. 8. The insects were attracted to the light source and screen. Although they were typically unobtrusive to the shadowgraphy, they have the potential to disrupt it if they fly too close to the optics, thus causing significant image blur. This probability is low, but the possibility should be considered, especially for complex setups observing only a one-shot experiment.

Another series of large-scale field experiments was performed with a portable retroreflective shadowgraph system at the Fire Safety Test Enclosure of the US Army's Aberdeen Test Center in Maryland. These experiments used the same optical components and camera as described above, but used a 5 m square retroreflective screen mounted against a steel backing. The light source and camera were positioned approximately 16 m from the screen, inside an armored enclosure. This enclosure required air conditioning to prevent heat buildup, especially in the case of the arc lamp.

Of many experiments conducted during this four-day field excursion, two examples are presented here to exemplify the ability to use this system in full-scale experiments under adverse conditions. Figure 9 shows the explosion of (a) an RP-83 exploding-

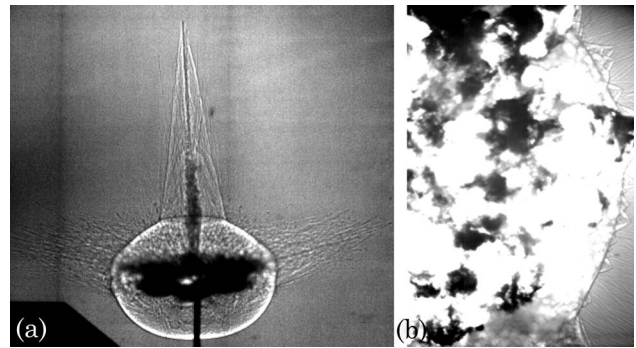


Fig. 9. (a) Image of an RP-83 detonator approximately $400\ \mu\text{s}$ after detonation and (b) a 0.45 kg C-4 charge about 1 ms after detonation, both with $1\ \mu\text{s}$ frame exposures.

bridgewire detonator and (b) a 0.45 kg C-4 plastic explosive.

The RP-83 detonator is a standard exploding-bridgewire detonator commonly used to initiate commercial and military explosives [20]. The detonator contains slightly more than a gram of high explosive (PETN and RDX) in a metal cylinder of 7 mm diameter and 40 mm length. The detonator was placed vertically in the experiment shown in Fig. 9(a), where the vertical field of view is approximately 1.2 m. The detonator is initiated from one end of the cylinder and hurls shrapnel primarily in the forward and radial directions. The metal end of the cylinder is projected upward in Fig. 9(a) at a particularly spectacular speed of about Mach 7 based on the angle of the attached shock wave.

Figure 9(b) is a shadowgram of the explosion of a 0.45 kg ball of bare C-4 plastic explosive ($\sim 91\%$ RDX by weight in a putty-like matrix [21]). The explosion center is near the middle of the left side of the field of view, which is cropped here to a length of approximately 1.2 m in the horizontal direction. The self-luminous fireball produced by the explosion partially overranges the camera here, due to the intensity of light produced. At the right edge of the fireball, however, the spherical blast wave is seen to emerge, punctuated by supersonic fragments.

Shadowgraphy of the C-4 explosion during the first millisecond was obscured by the direct light of the



Fig. 8. Image sequence of planar shock wave propagation from a fireworks display, impinging on the author (GSS). The shock appears defocused in the leftmost and rightmost images, while it is sharp in the center two images, due to its alignment with the diverging light rays of the shadowgraph illumination.

early fireball. This observation requires special considerations for experiments involving self-luminous objects within the test section. Any light produced by the schlieren object that is directed toward the camera or the screen has the potential to overranging the shadowgram. If detrimental to the experiment, the overranging can be limited by modifying camera settings such as exposure time, or by the use of neutral-density filters. A more effective solution would be to increase the shadowgraph illumination, thus overpowering the direct light from the schlieren object. This option could be implemented with the use of laser illumination and a notch filter, but was not attempted here.

C. Remington .30–06 High-Powered Rifle

A typical .30–06 high-powered rifle was used here to compare retroreflective shadowgraphy to schlieren imaging. The 2.4 m retroreflective screen, located 10 m from the camera and light source, was used here to obtain a field of view of about 1.2 m. Figure 10 shows a series of shadowgrams documenting the firing of the rifle, recorded with an interimage timing of $33 \mu\text{s}$ and an exposure of $1 \mu\text{s}$. The highly under-expanded supersonic jet of powder gases exits the rifle muzzle, propelling the bullet and driving a strong muzzle blast wave. The propellant gases form a toroidal vortex, and the bullet accelerates and emerges from this cloud moments later at a Mach number of about 2.5. Similar photographs were



Fig. 11. (Color online) Schlieren image of the firing of a Remington .30–06 high-powered rifle using the Penn State full-scale schlieren system.

published by Schardin [22], but with a smaller field of view.

The same rifle has also been examined by Settles and Dodson [23] using the Penn State full-scale schlieren system [1,24] and more recently by Hargather and Settles using background-oriented schlieren [13]. Figure 11 is a schlieren image of the same rifle being fired, taken using the Penn State full-scale schlieren system. When compared to the last image of Fig. 10, the differences between schlieren and shadowgraph visualizations can be observed. Schlieren visualizes the gradient of refractive index [1], revealing gradients inside the muzzle blast that are not seen in the corresponding shadowgram. The propellant gases are clearly visible in both images. The field of view for the present shadowgraphy

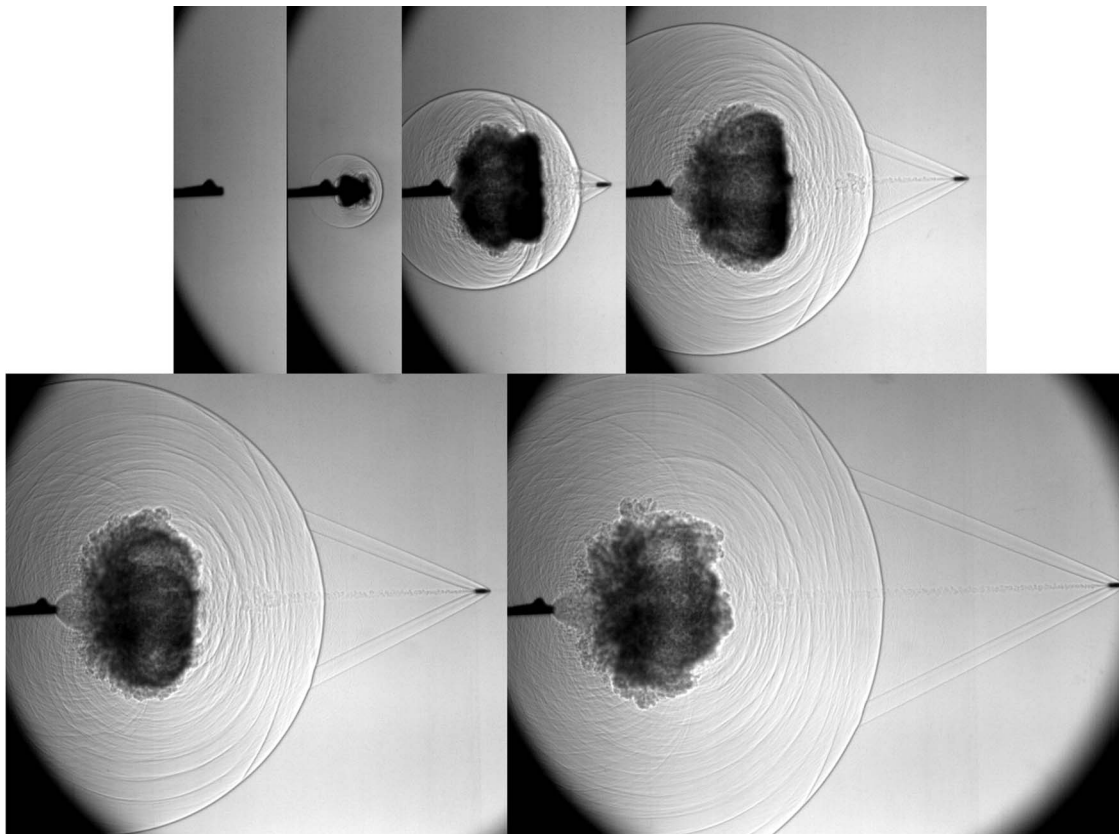


Fig. 10. Six consecutive shadowgrams of the firing of a Remington .30–06 high-powered rifle.

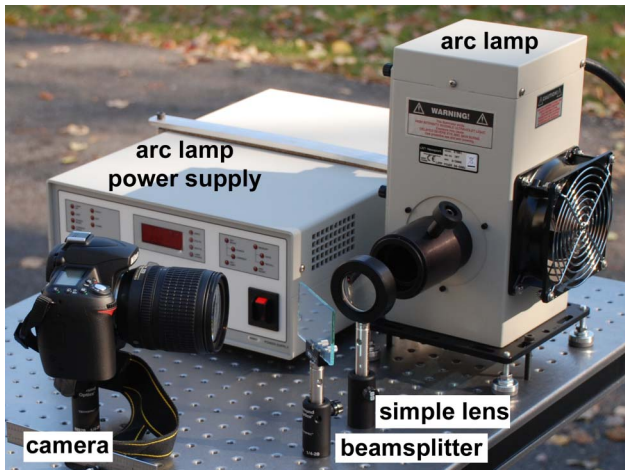


Fig. 12. (Color online) Optical setup used for thermal plume imaging.

was smaller than for the comparative schlieren image due to the size of the screen used, but could be expanded if required. Overall the two images are similar in all respects.

When comparing these visualization systems, note that the robustness and simplicity of the retroreflective shadowgraph system are much better than in the case of the lens-and-grid full-scale schlieren system. The retroreflective shadowgraph can be moved easily, including outdoors, which is not practical with a lens-and-grid schlieren system. The simple optics and screen construction of the retroreflective shadowgraph system also allow it to be applied at almost any scale, whereas many obstacles have to be overcome to build a schlieren system of equivalent size.

D. Thermal Plume Shadowgrams

For low-speed imaging of thermal plumes, the optical configuration using the beam splitter [Fig. 3(a)] is the simplest to implement. This arrangement has been easily combined with a 100 W arc lamp and a Nikon D90 digital camera and mounted on a single optical table to produce a complete instrument, as shown in Fig. 12. The 2.4 m retroreflective screen was positioned 8 m from the light source and camera for these experiments.

The thermal plume of a typical barbecue gas grill was observed here to show the sensitivity of the

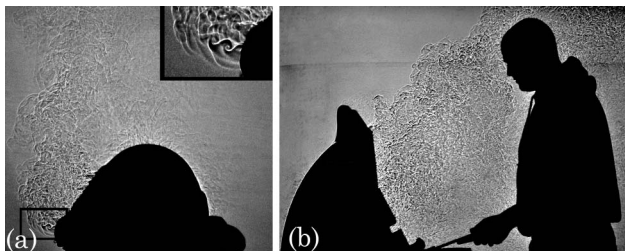


Fig. 13. Shadowgrams showing the thermal plume of a barbecue grill (a) with the top down and (b) up. The highlighted region of frame (a) is reproduced in the inset, showing Kelvin-Helmholtz vortices. A slight left-to-right breeze in frame (b) carries the thermal plume from the grill into the face of the author (MJH).

retroreflective shadowgraph technique. Two shadowgrams of the grill are shown in Fig. 13. These shadowgrams clearly show the hot, turbulent plume emanating from the grill. These experiments, conducted outdoors in full sunlight, further illustrate the robustness and range of operation of the retroreflective shadowgraph technique.

4. Conclusions

The simple but neglected retroreflective shadowgraph method of Harold E. “Doc” Edgerton has been revived and improved in the present work. This optical system has unique characteristics (simple optics, robust components, and high sensitivity) that make it well suited to experiments across a range of scales and environmental conditions.

The retroreflective shadowgraph method requires only a concentrated light source to project a shadowgram on a retroreflective screen and a camera to capture the shadowgram. Commercial light-source equipment and modern digital cameras are suitable for recording these shadowgrams. The simple optical alignment of these components does not require a high degree of accuracy for basic flow visualization, although precise alignment is recommended for quantitative data capture. The alignment process has been explored and improved here, including a discussion of three comparable methods for producing coincident illumination and camera images.

The range of applications for retroreflective shadowgraphy has been demonstrated for laboratory- and field-scale experiments using explosives, firearms, and low-speed thermal plumes. Although it is less sensitive and sophisticated than schlieren techniques, this shadowgraph method reveals shock waves and turbulent structures very effectively. These visualizations and the optical components are also insensitive to a range of environmental and weather conditions, including direct sunlight illumination.

The authors thank L. J. Dodson-Dreibelbis, J. A. Gatto, T. P. Grumstrup, J. D. Miller, and M. E. Staymates for their assistance. Some of this research was supported by FAA grant 99-G-032, now administered by the Department of Homeland Security (DHS). The mention of specific commercial products should not be seen as an endorsement by the DHS.

References

1. G. S. Settles, *Schlieren and Shadowgraph Techniques: Visualizing Phenomena in Transparent Media* (Springer-Verlag, 2001).
2. G. S. Settles, T. P. Grumstrup, L. J. Dodson, J. D. Miller, and J. A. Gatto, “Full-scale high-speed schlieren imaging of explosions and gunshots,” *Proc. SPIE* **5580**, 5580-174 (2005).
3. G. E. A. Meier, “Hintergrund schlierenmessverfahren,” Deutsche Patentanmeldung DE 199 42 856 A1 (1999).
4. H. E. Edgerton, *Electronic Flash, Strobe* (MIT Press, 1970).
5. H. E. Edgerton, “Shockwave photography of large subjects in daylight,” *Rev. Sci. Instrum.* **29**, 171–172 (1958).

6. J. K. Biele, "Point-source spark shadowgraphy at the historic birthplace of supersonic transportation—a historical note," *Shock Waves* **13**, 167–177 (2003).
7. S. P. Parthasarathy, Y. I. Cho, and L. H. Back, "Wide-field shadowgraphy of tip vortices from a helicopter rotor," *AIAA J.* **25**, 64–70 (1987).
8. T. R. Norman and J. S. Light, "Rotor tip vortex geometry measurements using the wide-field shadowgraph technique," *J. Am. Helicopter Soc.* **32**, 40–50 (1987).
9. A. Bagai and J. G. Leishman, "Improved wide-field shadowgraph set-up for rotor wake visualization," *J. Am. Helicopter Soc.* **37**, 86–92 (1992).
10. G. E. A. Meier, "Computerized background-oriented schlieren," *Exp. Fluids* **33**, 181–187 (2002).
11. L. Venkatakrisnan and G. E. A. Meier, "Density measurements using the background oriented schlieren technique," *Exp. Fluids* **37**, 237–247 (2004).
12. H. Richard and M. Raffel, "Principle and applications of the background oriented schlieren (bos) method," *Meas. Sci. Technol.* **12**, 1576–1585 (2001).
13. M. J. Hargather and G. S. Settles, "Natural-background-oriented schlieren," *Exp. Fluids* DOI:10.1007/s00348-009-0709-3 (2009).
14. 3M Industrial Adhesives and Tapes Division, 900 Bush Avenue, St. Paul, Minnesota, USA.
15. S. Winburn, A. Baker, and J. G. Leishman, "Angular response properties of retroreflective screen materials used in wide-field shadowgraphy," *Exp. Fluids* **20**, 227–229 (1996).
16. H. Kleine, J. M. Dewey, K. Ohashi, T. Mizukaki, and K. Takayama, "Studies of the TNT equivalence of silver azide charges," *Shock Waves* **13**, 123–138 (2003).
17. M. J. Hargather and G. S. Settles, "Optical measurement and scaling of blasts from gram-range explosive charges," *Shock Waves* **17**, 215–223 (2007).
18. M. J. Hargather, "Scaling, characterization and application of gram-range explosive charges to blast testing of materials," Ph.D. thesis (The Pennsylvania State University, 2008).
19. J. M. Dewey, "Explosive flows: shock tubes and blast waves," in *Handbook of Flow Visualization*, 1st ed. (Hemisphere, 1989), Chap. 29, pp. 481–497.
20. R. Varosh, "Electric detonators: EBW and EFI," *Propellants Explosives Pyrotechnics* **21**, 150–154 (1996).
21. P. W. Cooper, *Explosives Engineering* (Wiley-VCH, 1996).
22. H. Schardin, "Die schlierenverfahren und ihre anwendungen," *Ergeb. Exakten Naturwiss.* **20**, 303–439 (1942).
23. G. S. Settles and L. J. Dodson, "Full-scale schlieren visualization of supersonic bullet and muzzle blast from firing a .30–06 rifle," *J. Visualiz. Comput. Animation* **8**, 6 (2005).
24. G. S. Settles, "The Penn State full-scale schlieren system," in *Proceedings 11th International Symposium on Flow Visualization*, T. Mueller and I. Grant, eds. (IOP2004), paper 76.